Journal of Catalysis **185,** 265–271 (1999)
Article ID jcat.1999.2514, available online at http://www.idealibrary.com on IDEAL®

Influence of the Nature of the Exchanged Ion on *n*-Hexane Aromatization Activity of Pt–*M*–ETS-10: *Ab Initio* Calculations on the Location of Pt

S. B. Waghmode, T. K. Das, R. Vetrivel, and S. Sivasanker[1]

Catalysis Division, National Chemical Laboratory, Pune 411 008, India

Received December 15, 1998; accepted April 8, 1999

The activity of Pt–*M*–ETS-10 samples exchanged with different alkali metals (*M* = Li, Na, K, Rb, or Cs) in the aromatization of *n*-hexane depends on the nature of the exchanged metal ion (M). A distinct relationship between the intermediate electronegativity (S_{int}) of the different metal-exchanged ETS-10 samples and benzene yield is reported, suggesting the activation of Pt by the basicity of the exchanged metal. Results of *ab initio* Hartree–Fock calculations on cluster models representing Pt–*M*–ETS-10 corresponding to the presence of Pt nearer to $[TiO_6]^{2-}$ and $[SiO_4]$ groups reveal that the presence of Pt nearer to $[TiO_6]^{2-}$ is energetically more favored and results in a gain of electron charge by Pt. The studies also suggest an increasing amount of electron transfer from the model clusters of ETS-10 to the Pt with increase in the electropositive character of the exchanged metal. It appears therefore, that small Pt clusters residing nearer to $[TiO_6]^{2-}$ accessible from the 12-MR channels are the likely active sites in *n*-hexane aromatization over Pt–*M*–ETS-10.

INTRODUCTION

Though bifunctional catalysts such as Pt (with or without promoters) supported on acidic halided aluminas are the catalysts of choice for the aromatization of *n*-paraffins into aromatics (catalytic reforming) (1, 2), monofunctional catalysts such as Pt supported on the nonacidic zeolite K–L (3) and Mg(Al)O (4) have also been reported. The monofunctional catalysts have been reported to be many times more active than bifunctional catalysts in the reforming of *n*-paraffins with carbon numbers less than 9 (3). Besoukhanova *et al.* (5) have reported that the activity of Pt–L exchanged with different alkali metal ions in *n*-hexane aromatization increases with increasing basicity of the alkali metal, viz., Li < Na < K < Rb < Cs. Das *et al.* (6) have made a similar observation in their study of *n*-hexane aromatization over Pt supported on different alkali metal-exchanged ETS-10. Similarly, Philippou *et al.* (7) have also reported high benzene yields over Pt–K–ETS-10 and Pt–K–ETAS-10 in the aromatization of *n*-hexane.

[1] To whom correspondence should be addressed. FAX: +91-20-589 3761. E-mail: siva@cata.ncl.res.in.

Barthomeuf (8) has reported an inverse relationship between benzene yield in the aromatization of *n*-hexane and the intermediate electronegativity (S_{int}) (9) of Pt–L zeolite exchanged with different alkali metal ions. S_{int} is inversely related to the charge on the O^{2-} ions the latter being a measure of the basicity of the zeolite. The net conclusion of the above studies (5–8) is that there is a transfer of electronic charge from the O^{2-} ions of the basic supports to the Pt clusters making them electron rich. The electron-rich Pt clusters present on nonacidic supports are more active in the aromatization of *n*-paraffins than the Pt clusters present on acidic supports.

In this paper, we report our studies on the influence of alkali metal ions on the activity of Pt–ETS-10 on *n*-hexane aromatization. Molecular modeling methods and *ab initio* calculations have been used to examine the electronic properties of Pt in different locations of Pt–M–ETS-10 catalysts. The likely location of the active Pt species is identified.

EXPERIMENTAL

Sample Preparation and Reaction Studies

ETS-10 was prepared according to the procedure reported earlier (10). The different ion-exchanged samples were prepared by repeated exchanges with the required salt solution. Information on the Pt-loading procedure, characterization of the samples, and reaction and analysis details have also been reported elsewhere (6).

Methods of Calculation and Models Used

The *ab initio* calculations have been performed at the Hartree–Fock level. Since all the neutral systems considered in this study are closed shells, Restricted Hartree–Fock (RHF) calculations have been used. The *ab initio* calculations have been performed using an effective core potential (ECP) according to Stevens *et al.* (11–13). Computations were carried out using the General Atomic and Molecular Electronic Structure System (GAMESS) package (14) in a SiliconGraphics O_2 workstation. ETS-10 is a large-pore titanosilicate molecular sieve that was first synthesized at

0021-9517/99 $30.00

TABLE 1

Interatomic Distance Values Used in the Present Calculations

Atom-to-atom distance	Distance (Å)
Pt–Pt	2.77
Ti–O (planar)	1.89[a]
Ti–O (axial)	1.91[a]
Si–O	1.55–1.59[a]
Li–O	2.16
Na–O	2.42
K–O	2.78
Rb–O	2.92
Cs–O	3.07

[a] As derived from the crystal structure reports (16).

Engelhard (15). The framework structure of ETS-10 consists of corner-shared oxygen ions of $[TiO_6]^{2-}$ octahedra and $[SiO_4]$ tetrahedra. The cluster models of ETS-10 have been derived from the crystal structure of ETS-10–polymorph B (unit cell: $\{[M^+]_{32}\ [(TiO_3)^{2-}]_{16}[SiO_2]_{80}\}$, where $M^+ = Li^+$, Na^+, K^+, Rb^+, or Cs^+) reported by Anderson *et al.* (16, 17). The projection of ETS-10 lattice as viewed through the 110 plane is shown in Fig. 1. The structure is made up of interconnected rings of 3, 4, 5, 7, and 12 members. The geometry of the platinum cluster was derived from the crystal structure of Pt (FCC lattice). The cluster models were generated using the software packages InsightII (supplied by Molecular Simulations, Inc., USA) and SPARTAN (supplied by Wavefunction, Inc., USA). Table 1 shows the interatomic distances used in the *ab initio* calculations. *M*–O distances are the sum of the ionic radii of M^+ and O^{2-}. The influence of the location and orientation of the Pt inside the pores of ETS-10 on its (Pt) electronic properties was examined.

RESULTS AND DISCUSSION

The reasons for the superior aromatization selectivity of Pt–L have been investigated by many authors. Both steric and electronic factors have been invoked. Tauster and Steger (18) have proposed that the pore openings in zeolite L collimate diffusing *n*-hexane molecules, leading to end-on adsorption on the Pt clusters situated inside the cancrinite cages of zeolite L. Such an end-on adsorption should facilitate 1,6 ring closure leading to aromatization. Newsam *et al.* (19) believe that the steric constraints imposed by the surrounding cage should be responsible for promoting conformations of *n*-hexane molecules (already terminally bonded to Pt atoms) that will lead to 1,6 ring closure. However, they have indicated that preferred Pt atom sites at high dispersion remain unmeasured inside Pt–L. Derouane and Vanderveken (20), on the basis of molecular modeling studies, have proposed a *confinement model*, the essence of which is that an *n*-hexane molecule diffusing inside the barrel-shaped channels forms a pseudo cycle by attachment of the terminal carbon to a Pt atom (or a Pt cluster) present in an adjacent cancrinite cage followed by curving of the molecule. This cyclic intermediate formation is assisted by the pore architecture of zeolite L. The intermediate transforms into benzene through C–C bond formation and dehydrogenation. Based on their studies of the conversion of *n*-hexane over Pt–Y zeolites and Pt–L zeolites, Lane *et al.* (21) have also concluded that the confinement model offers a better explanation for the superior aromatization activity of Pt–L. However, Iglesia and Baumgartner (22) have postulated that the good performance of Pt–L zeolite in aromatization is due to the LTL pore system offering protection to the Pt clusters from carbon deposition.

As mentioned earlier, Besoukhanova *et al.* (5) have related the aromatization activity of Pt supported on various L zeolites to the increasing basicity of the exchanged metal ions. Furthermore, based on infrared shifts of CO adsorbed on Pt in these catalysts, the Pt particles were shown to be electron rich, the electron richness of the Pt clusters arising from interaction with the basic O^{2-} ions in the lattice. It has been suggested (5, 8, 23) that the high activity of Pt–L is due to the electron-rich nature of the Pt supported on it. This explains better the high *n*-hexane (3) aromatization activity of Pt supported on different zeolites with different pore architectures (3) and even amorphous oxides such as Mg(Al)O and alkali-poisoned Al_2O_3 (21), though additional beneficial effects of steric factors and lower deactivation can not also be ignored in some cases. Why exactly an electron-rich Pt is more selective is not clear, though it could be due to greater ease of desorption of the aromatic compound (5). In this study, we demonstrate through *ab initio* calculations that distinct transfer of electrons to the Pt occurs in Pt–ETS-10, especially when it is located in specific locations in the 12-MR pores.

Aromatization of n-Hexane over Pt–M–ETS-10

The *n*-hexane aromatization activities of a series of Pt–*M*–ETS-10 containing exchanged alkali metal ions are presented in Table 2 (6). It is noticed that the more basic catalysts were more active in *n*-hexane aromatization. The benzene selectivity also shows a similar trend. The activity increases with the increase in the electropositive nature of the exchanged metal in the order Li < Na < K < Rb < Cs. As reported by Barthomeuf in the case of Pt–L (8), the benzene yields obtained over the Pt–*M*–ETS-10 samples (6) also can be correlated to their intermediate electronegativities and the negative charge on the oxygen ion as shown in Fig. 2. It appears therefore that in the case of Pt–*M*–ETS-10, also, the enhancement of aromatization activity with increasing basicity of the alkali ions is due to increasing electron flow from the support to the metal and the Pt clusters are electron rich as reported in the case of Pt–L.

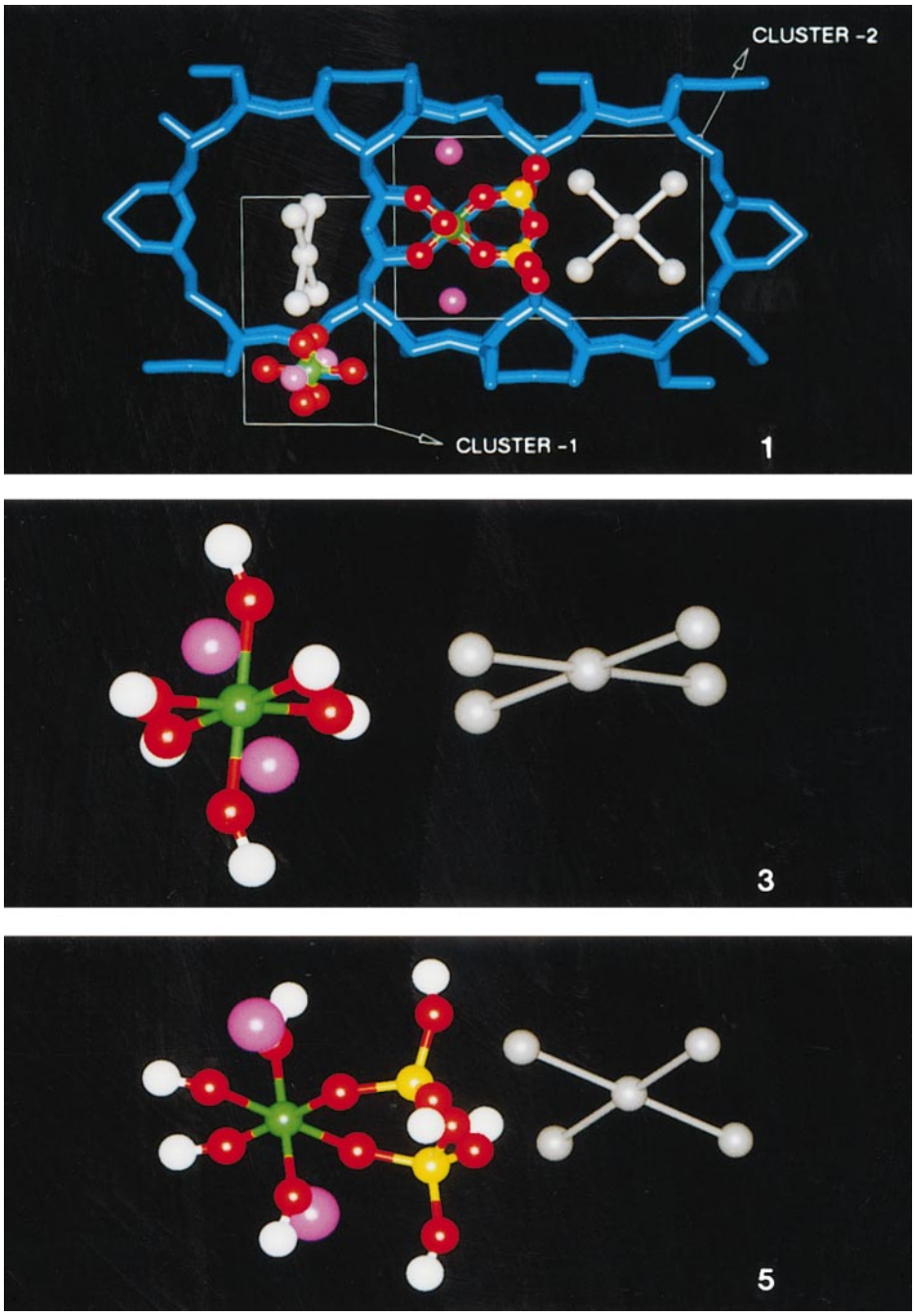

FIG. 1. Molecular graphics picture of ETS-10 lattice, as viewed along the 110 plane. The cluster models representing the presence of Pt_5 nearer to $[TiO_6]^{2-}$ and $[SiO_4]$ groups are highlighted. Blue stick model indicates the ETS-10 framework; Pt, grayish white; Ti, green; Si, yellow; O, red, and M, pink.

FIG. 3. The molecular graphics picture of the $Ti(OH)_6M_2 : Pt_5$ (where $M =$ Li, Na, K, Rb, or Cs) cluster model. This cluster represents the presence of Pt_5 nearer to $[TiO_6]^{2-}$. Among the two possible (parallel and perpendicular) orientations for Pt_5, the energetically favorable parallel orientation is shown. Pt, grayish white; Ti, green; O, red; M, pink, and H, white.

FIG. 5. The molecular graphics picture of the $TiSi_2O_3(OH)_8M_2 : Pt_5$ (where $M =$ Li, Na, K, Rb, or Cs) cluster model. This cluster represents the presence of Pt_5 nearer to $[SiO_4]$. Among the two possible (parallel and perpendicular) orientations for Pt_5, the energetically favorable parallel orientation is shown. Pt, grayish white; Ti, green; Si, yellow; O, red; M, pink; and H, white.

TABLE 2

***n*-Hexane Aromatization over Pt–*M*–ETS-10 (6)**

Catalyst	Pt–*M*–ETS-10[a] (0.4 wt% Pt), where *M* =				
	Li	Na	K	Rb	Cs
n-Hexane conversion (wt%)	11.7	17.2	27.2	47.0	84.8
Benzene selectivity (%)	5.1	5.2	14.0	30.8	34.5
Product distribution (wt%)					
C_1	0.2	0.4	0.8	2.1	7.0
C_2	0.5	1.0	1.3	1.6	1.8
C_3	0.6	1.4	1.8	1.4	1.8
C_4[b]	0.4	0.5	1.2	1.7	4.7
C_5[c]	0.1	0.1	0.7	3.0	16.4
i-C_6[d]	0.7	0.3	1.0	3.2	12.2
$McyC_5$[e]	0.1	0.4	0.7	1.5	5.4
Benzene	0.6	0.9	3.8	14.5	29.3
C_6^+ aromatics[f]	—	—	0.1	0.1	0.1
Others	8.5	12.2	15.8	17.9	6.1

[a] Reaction conditions: WHSV = 2 h^{-1}; pressure = 1 atm; TOS = 2 h; H_2 : *n*-hexane (mole) = 4 : 4; temperature = 723 K.
[b] C_4 = *i*-butane + *n*-butene.
[c] C_5 = *i*-pentane + *n*-pentene.
[d] *i*-C_6 = 2,2-dimethylbutane + 2,3-dimethylbutane + 2-dimethylpentane + 3-methylpentane.
[e] $McyC_5$ = methyl cyclopentane.
[f] C_6^+–Aromatics = toluene + xylenes.

Electronic Structure of Pt in Pt–M–ETS-10

We have modeled the Pt atom (cluster) in different locations of Pt–M–ETS-10 by suitable cluster models. The major pores in ETS-10 are the 12-MR channels (Fig. 1). These channels are intersected by smaller 7-, 5-, and 3-MR channels in such a way that the walls of the 12-MR channels are linked by pockets of 7-, 5-, 4-, and 3-MR openings. The Ti atoms are accessible through pore openings, some of which are blocked by the exchanged alkali metal ions (24). There are several possible locations for Pt in Pt–*M*–ETS-10. Given the large size of a Pt atom (2.77 Å), atomically dispersed Pt atoms and small Pt clusters can be present only inside the 7-MR (~3 Å) and 12-MR (~8 Å) openings. The Pt atoms (or clusters) present inside the 12-MR channels will be directly accessible to the diffusing *n*-hexane molecules. Single Pt atoms present inside the 7-MR may also be accessible to the reactant molecules through the 12-MR channels only in their end-on orientation due to the small size (~3 Å) of the 7-MR openings. This structural fitting analysis lead to the conclusion that Pt in 7-MR cages may be available only to terminal carbons, while a Pt atom or small clusters of Pt such as Pt_5 present inside the 12-MR pores will be more accessible to the entire molecule. However, the presence of alkali ions inside the 7-MR channels restricts the possibility of Pt atoms being present in them. More over, as it is difficult even for the terminal carbon of *n*-hexane to enter the 7-MR pockets (let alone its forming a cyclic ring), we believe these Pt atoms (if present) are less likely to be the active species for aromatization. We have therefore examined the two possible locations of Pt inside the 12-MR and its interaction with the (*M*)–ETS-10, as shown in Fig. 1.

A single platinum atom and Pt clusters containing several atoms were considered. Initial trial calculations were performed using the Extended Huckel method of Hoffmann (25) using the Computer Aided Composition of Atomic Orbital (CACAO) package (26). The geometry of Pt_n clusters (where $n = 2$ to 9) was derived from the FCC crystal data of platinum. As we go from a single Pt atom to a Pt_5 cluster, there is a drastic variation in the electronic properties. However Pt_5 to Pt_9 have the same order of binding energy and similar electronic properties (27). The dimension of a Pt_5 square planar cluster is 5.54×5.54 Å, which can ideally fit inside the 12-MR channels of ETS-10. The small concentration of Pt (0.4 wt%) and the good dispersion values of 0.45 to 0.73 in the Pt–*M*–ETS-10 samples suggest that a significant portion of Pt exists as dispersed atoms or small clusters. Hence, we studied the electronic structure of monomeric Pt and a small cluster (Pt_5) inside ETS-10. The results obtained for both a single Pt and a Pt_5 cluster in different locations inside *M*-ETS-10 were found to be essentially similar. However, the electronic properties of the monomeric Pt atom were extremely

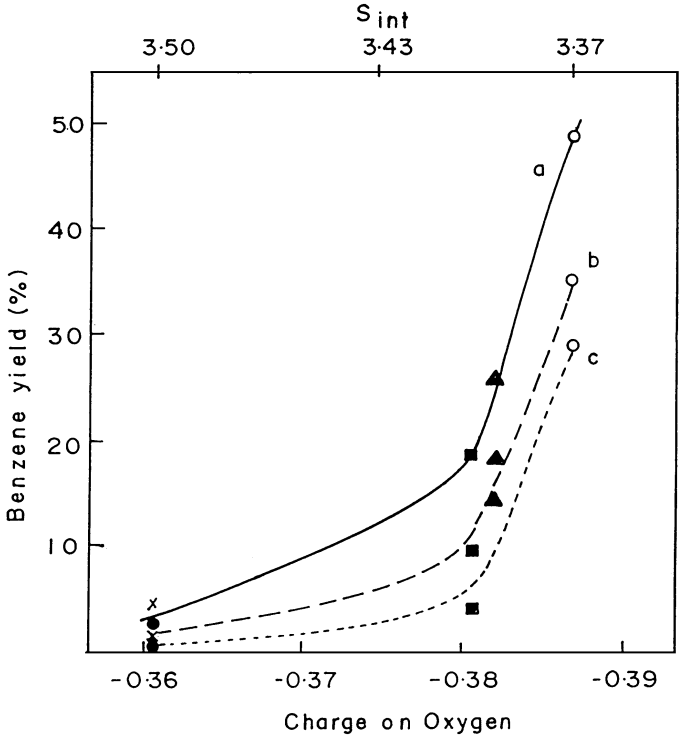

FIG. 2. Benzene yield in *n*-hexane aromatization as a function of S_{int} and oxygen charge of Pt(0.4%)–ETS-10 samples exchanged with (●) Li–ETS-10, (×) Na–ETS-10, (■) K-ETS-10, (▲) Rb–ETS-10, and (○) Cs–ETS-10. (a) 773 K, (b) 748 K, and (c) 723 K.

TABLE 3

The Electronic Properties of the Cluster Model Where Pt Is Nearer to $[TiO_6]^{2-}$

Clusters *M*	$[M_2Ti(OH)_6]$ Total energy (a.u.)	$[M_2Ti(OH)_6]$ Net electron charge on M^a	$[M_2Ti(OH)_6:Pt_5]$ Total energy (a.u.)	Binding energy^b (kcal/mol)	Net electron charge on Pt^a	Net electron charge on M^a
Li	−155.6862	0.6615	−749.7709	−13.4912	−0.0207	0.7074
Na	−155.6081	0.8041	−749.7065	−22.0880	−0.0224	0.8089
K	−155.5242	0.9195	−749.6431	−36.8970	−0.0276	0.9456
Rb	−155.5211	0.9623	−749.6539	−43.6740	−0.0328	0.9656
Cs	−155.4827	0.9625	−749.6172	−44.7407	−0.0325	0.9649

[a] Average charge on platinum and alkali metal.
[b] B.E. = T.E. $[M_2Ti(OH)_6:Pt_5]$ − {T.E. $[M_2Ti(OH)_6]$ + T.E. $[Pt_5]$}.

sensitive to the location, i.e., the distance from the ETS-10 *surface* (27), while in the case of Pt_5 the variations were gradual. All the results presented hereafter are for Pt_5 clusters interacting with the *M*–ETS-10 system. Two likely (distinctly different) locations of a Pt_5 cluster inside the 12-MR were considered, one in proximity to the $[TiO_6]^{2-}$ (Fig. 1, cluster 1) and another in proximity to the $[SiO_4]$ (Fig. 1, cluster 2).

Electronic Structure of Pt Nearer to TiO_6

The cluster model (Fig. 1, cluster 1) representing this situation is shown in Fig. 3. and the stoichiometry is $M_2Ti(OH)_6:Pt_5$. The unsaturated valency of oxygens in TiO_6 is saturated by bonding a hydrogen to each of the oxygen atoms. The O–H distance used was 1.03 Å with the O–H vector lying along the original O–Si vector in the ETS-10 lattice from which the TiO_6 cluster was created. Several orientations of Pt_5 were considered, while the alkali metal cations were sited at locations predicted by EXAFS (24). The Pt_5 plane oriented perpendicular to the 110 plane as shown in Fig. 3 was found to be energetically most favorable. The electronic properties of $M_2Ti(OH)_6$ were derived by systematically varying *M* from Li to Cs. The results of *ab initio* calculations given in Table 3 indicate that the positive charge on *M* increases in the order Li < Na < K < b ≅ Cs. The highest occupied molecular orbitals (HOMO) are contributed by oxygen 2*p* atomic orbitals while the lowest unoccupied (LUMO) are contributed by the *p* orbitals of *M* and 1*s* atomic orbitals of *H*. When Pt_5 was introduced, the Pt–ETS-10 interactions were studied by performing *ab initio* calculations on $M_2Ti(OH)_6:Pt_5$ cluster models. The binding energy of Pt_5 with $[TiO_6M_2]$ clusters was calculated as shown below and is presented in Table 3.

$$\text{B.E.} = \text{T.E.}\,[M_2Ti(OH)_6:Pt_5] - \{\text{T.E.}\,[M_2Ti(OH)_6] + \text{T.E.}\,[Pt_5]\}. \quad [1]$$

The following observations are made from the results of these calculations presented in Table 3 (and Fig. 4).

1. The interaction of Pt_5 with *M*–ETS-10 increases with the electropositive nature of the exchanged ion (Li < Na < K < Rb < Cs).
2. The electron density on Pt in these cluster models also increases in the order Li < Na < K < Rb ≅ Cs as does the positive charge on the exchanged metal atoms themselves.

The absolute values of the binding energy values may not carry much chemical meaning due to the small cluster models considered here. However, the trend is clearly predicted. The binding energy values take care of the charge as well as the size of the *M* cation. When the net charges on Pt and *M* are calculated by the Mulliken population, the Pt–Cs– ETS-10 cluster model does not follow the same trend as the other ions; the electron charge is slightly less than Rb (Fig. 4). In the case of Cs, the empty 4*f* and 5*f* orbitals are expected to be more diffused, leading to an increase in the volume and a consequent decrease in charge per unit volume.

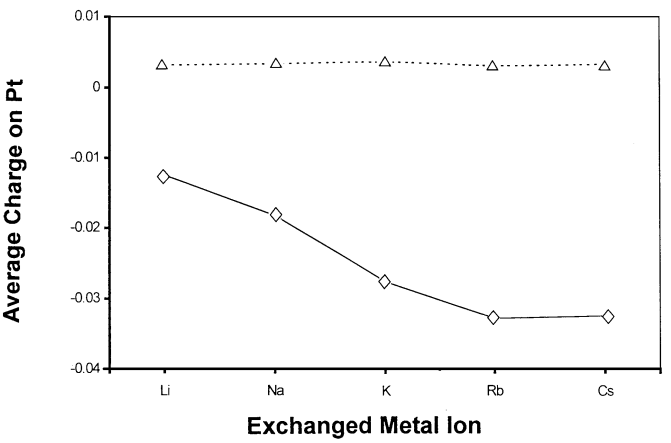

FIG. 4. The variation of average charge on platinum in the Pt_5 cluster when it is located nearer to $[TiO_6]^{2-}$ (◇) and nearer to $[SiO_4]$ (△) with the nature of exchanged ion.

TABLE 4

The Electronic Properties of the Cluster Model Where Pt Is Nearer to [SiO_4]

Clusters M	$[M_2TiSi_2O_3(OH)_8]$ Total energy (a.u.)	$[M_2TiSi_2O_3(OH)_8]$ Net electron charge on M^a	$[M_2TiSi_2O_3(OH)_8:Pt_5]$ Total energy (a.u.)	Binding energy^b (kcal/mol)	Net electron charge on Pt^a	Net electron charge on M^a
Li	−242.9197	0.6921	−836.9932	−7.2790	0.0032	0.6905
Na	−242.8483	0.8280	−836.9225	−7.8437	0.0034	0.8303
K	−242.7697	0.9304	−836.8461	−8.7222	0.0037	0.9306
Rb	−242.7629	0.9686	−836.8397	−9.1615	0.0031	0.9703
Cs	−242.7308	0.9666	−836.8087	−9.5380	0.0033	0.9649

[a] Average charge on platinum and alkali metal.
[b] B.E. = T.E. $[M_2TiSi_2O_3(OH)_8:Pt_5]$ − {T.E. $[M_2TiSi_2O_3(OH)_8]$ + T.E. $[Pt_5]$}.

Eelectronic Structure of Pt Nearer to SiO_4

The cluster model (Fig. 1, cluster 2) representing this situation is shown in Fig. 5 and the stoichiometry is $M_2TiSi_2O_3(OH)_8$. The *ab initio* calculations were performed as in the earlier case. The Pt_5 plane oriented parallel to the 110 plane is found to be energetically favorable.

The results of these calculations are shown in Table 4 (and Fig. 4). It can be observed that the positive charge on M is comparable to the charges given in Table 3, despite the fact that these are larger cluster models. These results indicate that the electron distribution is a localized phenomenon. The binding energy values calculated for these clusters according to the formula shown below are also presented in Table 4.

$$\text{B.E.} = \text{T.E.}\,[M_2TiSi_2O_3(OH)_8:Pt_5] - \{\text{T.E.}\,[M_2TiSi_2O_3(OH)_8] + \text{T.E.}\,[Pt_5]\} \quad [2]$$

Though the binding energy values increase with increase in electropositive nature of the exchanged metal, the values are smaller than those observed for cluster 1 (Table 3). This indicates that the preferred location of Pt is nearer to TiO_6 rather than to SiO_4. The net charges on Pt when present closer to Si are closer to zero and are slightly positive (Table 4). Based on the experimental data and the above calculations, it appears that the Pt and then the Pt atoms closer to the Ti are likely to be the more active ones for *n*-hexane aromatization.

CONCLUSIONS

Both *n*-hexane aromatization activity and benzene selectivity increase with increasing basicity of the alkali metal in Pt–*M*–ETS-10. Benzene yield is found to be a function of the intermediate electronegativity (S_{int}) of the *M*–ETS-10, suggesting an increasing transfer of electronic charge from the basic support to the metal with increasing electropositive character of the alkali metal. The charge polarization calculated by *ab initio* calculations also follows the experimental trends. Thus, in the case of Pt–*M*–ETS-10, electron transfer from the basic support to the Pt is probably the main reason for its excellent *n*-hexane aromatization activity as already reported in the case of Pt–K–L (3, 5) and Pt–Mg(Al)O (4).

The electron transfer from the support to the Pt occurs more effectively when the Pt is located nearer to $[TiO_6]^{2-}$ rather than to SiO_4. The interaction between $[TiO_6]^{2-}$ and Pt is also more favorable than that between SiO_4 and Pt. Thus, there is a clear preference of location for the Pt inside *M*-ETS-10 pores in the proximity of $[TiO_6]^{2-}$.

ACKNOWLEDGMENT

The authors acknowledge the financial support of the Department of Science and Technology, New Delhi, through the UK–India Science and Technology Research Fund.

REFERENCES

1. Antos, G. J., Aitani, A. M., and Parera, J. M. (Eds.), "Catalytic Naphtha Reforming, Science and Technology." Dekker New York, 1995.
2. Sinfelt, J. H., *in* "Catalysis Science and Technology" (J. R. Anderson and M. Boudart, Eds.), Vol. 1, p. 257. Springer-Verlag, Berlin, 1981.
3. Bernard, J. R., *in* "Proceedings, 5th International Conference on Zeolites" (L. V. C. Rees, Ed.), p. 686. Heyden, London, 1980.
4. Davis, R. J., and Derouane, E. G., *Nature* **349**, 313 (1991).
5. Besoukhanova, C., Guidot, J., Barthomeuf, D., Breysse, M., and Bernard, J. R., *J Chem. Soc. Faraday Trans. I* **77**, 1595 (1981).
6. Das, T. K., Chandwadkar, A. J., and Sivasanker, S., *Stud. Surf. Sci. Catal.* **113**, 455 (1998); Das, T. K., "Synthesis, Characterization and Catalytic Properties of Microporous Titanosilicate Molecular Sieves," Ph.D. thesis, Poona University, February, 1997.
7. Philippou, A., Naderi, M., Pervaiz, N., Rocha, J., and Anderson, M. W., *J. Catal.* **178**, 174 (1998).
8. Barthomeuf, D., *Stud. Surf. Sci. Catal.* **65**, 157 (1991).
9. Mortier, W. J., *J. Catal.* **55**, 138 (1978).
10. Das, T. K., Chandwadkar, A. J., and Sivasanker, S., *J. Chem. Soc. Chem. Commun.* 1105 (1996).

11. Stevens, W. J., Basch, H., and Krauss, M., *J. Chem. Phys.* **81**, 6026 (1984).
12. Stevens, W. J., Basch, H., Krauss, M., and Jasien, P., *Can. J. Chem.* **70**, 612 (1992).
13. Cundari, T. R., and Stevens, W. J., *J. Chem. Phys.* **98**, 5555 (193).
14. Schmhidt, M. W., Baldridge, K. K., Boatz, J. A., Elbert, S. T., Gordon, M. S., Jensen, J. H., Koseki, S., Matsunga, N., Nguyen, K. A., Su, S. J., Windus, T. L., Dupuis, M., and Montgomery, J. A., *J. Comput. Chem.* **14**, 1347 (193).
15. Kuznicki, S. M., U.S. Patent No. 5,011,591, 1991.
16. Anderson, M. W., Terasaki, O., Ohsuna, T., Philippou, A., Mackay, S. P., Ferreira, A., Rocha, J., and Lidin, S., *Nature.* **367**, 347 (1994).
17. Anderson, M. W., Terasaki, O., Ohsuna, T., Malley, P. J. O., Philippou, A., Mackay, S. P., Ferreira, A., Rocha, J., and Lidin, S., *Philos. Mag. B* **71**, 813 (1995).
18. Tauster, S. J., and Steger, J. J., *J Catal.* **125**, 387 (1990).
19. Newsam, J. M., Silbernagel, B. G., Garcia, A. R., Melchior, M. T., and Fung, S. C., *Stud. Surf. Sci. Catal.* **67**, 211 (1990).
20. Derouane, E. G., and Vanderveken, D. J., *Appl. Catal. A* **45**, L15 (1988).
21. Lane, G. S., Modica, F. S., and Miller, J. T., *J. Catal.* **129**, 145 (1991).
22. Iglesia, E., and Baumgartner, J. E., *in* "Proceedings, 10th International Congress on Catalysis Budapest, 1992" (L. Guczi, F. Solymosi, and P. Tetenyi, Eds.), Part B, p. 993. Akadémiai Kiadó, Budapest, 1993.
23. Larsen, G., and Haller, G. L., *Catal. Lett.* **3**, 1003 (1989).
24. Sankar, G., Bell, R. G., Thomas, J. M., Anderson, M. W., Wright, P. A., and Rocha, J., *J. Phys. Chem.* **100**, 449 (1996).
25. Hoffmann, R., *J. Chem. Phys.* **39**, 1397 (1963).
26. Mealli, C., and Proserpio, D. M., *J. Chem. Edu.* **67**, 399 (1990).
27. Waghmode, S. B., Vetrivel, R., and Sivasanker, S., unpublished results.